IEEE Photonics Journal
An IEEE Photonics Society Publication

Material Clustering Using Passive Millimeter-Wave Polarimetric Imagery

Volume 11, Number 1, February 2019

Jinlong Su
Yan Tian
Fei Hu
Yayun Cheng
Yan Hu

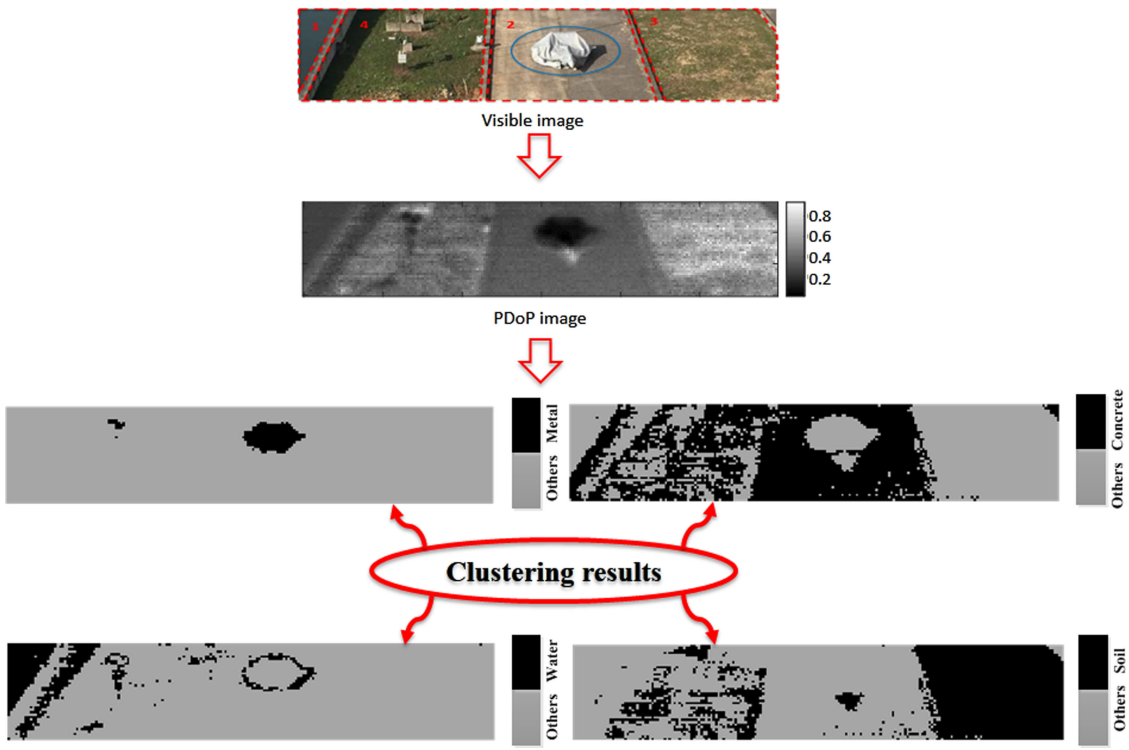

DOI: 10.1109/JPHOT.2018.2881287
1943-0655 © 2018 CCBY

Material Clustering Using Passive Millimeter-Wave Polarimetric Imagery

Jinlong Su,[1] **Yan Tian**,[1,2] **Fei Hu**,[1,2] **Yayun Cheng**,[1] **and Yan Hu**[1]

[1]School of Electronic Information and Communications, Huazhong University of Science and Technology, Wuhan 430074, China
[2]National Key Laboratory of Science and Technology on Multi-Spectral Information Processing, Wuhan 430074, China

DOI:10.1109/JPHOT.2018.2881287

Manuscript received October 8, 2018; revised November 3, 2018; accepted November 10, 2018. Date of publication November 14, 2018; date of current version December 24, 2018. This work was supported in part by the Fundamental Research Funds for the Central Universities under Grant HUST:2017JYCYJJ036. Corresponding author: Yan Tian (email: tianyan@hust.edu.cn).

Abstract: Passive millimeter-wave imaging has emerged as a useful tool in many remote sensing applications, including resource remote sensing, material classification, and target detection. This paper presents a method to classify specular objects based on their material composition from passive millimeter-wave polarimetric imagery. Passive degree of polarization (PDoP) is proposed and calculated by using the results of a passive millimeter-wave polarization measurement. The PDoP values of typical ground targets are further analyzed. Outdoor experiments are conducted, and the PDoP image is generated from the brightness temperature images. The PDoP values of pixels in the image are statistically analyzed, and the threshold values are set based on the statistical analysis results, then every pixel is recognized. Experimental results indicate that this method is highly effective for distinguishing among various materials of interest.

Index Terms: Passive millimeter-wave, passive degree of polarization, clustering.

1. Introduction

Passive millimeter-wave (PMMW) technology is continuing to improve due to several commercial drivers, notably in the agricultural remote sensing [1]–[3], security industries [4], [5] and military application [6]–[8]. PMMW sensors provide penetrability through a variety of low-visibility conditions, where textiles, smoke, fog, light rain, and dust storms exist. While PMMW technology without active illumination is useful in some military applications due to its covert operation, PMMW sensors have been proposed to be used in a variety of situations, such as helicopter landing and explosives detection. This increases the contrast of outdoor imagery for PMMW sensors since reflective materials will have lower radiometric temperatures compared to non-reflective materials, and the former has radiometric temperatures closing to ambient temperatures. All these characteristics of PMMW technology lead to easier automated target detection with fewer false alarms. PMMW imaging forms images through the passive detection of naturally occurring millimeter-wave radiation from a scene. It has extensive applications in military missions and civilian missions, including precision targeting, terminal guidance for missile, aircraft landing, search and rescue, security check, and concealed weapons detection in airports and other locations. In PMMW images, the values of apparent temperature are displayed in each pixel, the apparent temperature of the target

is determined by emissivity, the physical temperature, and the ambient temperature. Thus, the PMMW images are not enough to identify the target in the scene directly.

Polarization is a feature of electromagnetic radiation that conveys information about target material, surface features, shapes, local curvature and roughness. Polarimetric measurement has been widely used in acquiring additional information that includes index of refraction and reflection angle estimation [9]–[11], and surface geometry inspection [12], [13].

A lot of works on the utility of passive polarimetry for remote sensing applications have been published. Wolff [14] proposed a method to distinguish metals and dielectrics by recording the polarization state of reflected light using a passive polarimeter. Polarization Fresnel Ratio (PFR), which is the ratio of perpendicular to parallel polarization state components, is involved in his method. Thilak *et al.* [11] presented a method to jointly estimate the complex index of refraction and the reflection angle of specular targets from a set of passive polarization measurements made in the visible range of the spectrum. Degree of Polarization (DoP) is used as the feature discriminator to describe the polarization characteristics of the target in this method. There are also other feature discriminators in the existing literature, including degree of linear polarization (DoLP), degree of circular polarization (DoCP), multispectral polarimetric methods and so on [15]. However, these methods usually require lighting sources. Wilson *et al.* [16] utilized the difference of radiometric temperature for the two orthogonal linear polarization states to identify the PMMW images. In our previous works, we propose the mixed dielectric constant (MDC) to stand for the dielectric constant and offer a corresponding calculation method of MDC in passive microwave radiation related application [9]. Based on the forward model simulations, we define a parameter named Ratio of Angle-Polarization Difference (RAPD), which is a specific value of the horizontally polarized brightness temperatures (BTs) difference of two observation angles to the vertically polarized BTs difference of the same two observation angles. In addition, Linear Polarization Ratio (LPR) was presented to identify metal and dielectrics [17].

In this paper, Passive Degree of Polarization (PDoP) which is similar to the DoP in the visible and infrared range of the spectrum is proposed as a feature discriminator in PMMW measurement. The PDoP characteristics of several typical materials in millimeter-wave band are analyzed and an outdoor experiment is conducted. The distribution of PDoP values of the experiment scene is counted. The thresholds are automatically obtained by the minimum within-class distance criterion and applied to cluster pixels in the PDoP image. The material types of each cluster are defined through comparing the mean values of each cluster with the theoretical PDoP values of each material.

2. Basic Theory

Each body whose temperature is above absolute zero (0 K) emits radiation. As a result of the impact between the atoms and molecules, all matters naturally radiate electromagnetic energy. The radiance emitted by an object in millimeter wave bands can be approximated as a function of physical temperature by Rayleigh-Jeans approximation. Kirchhoff's law denotes that for an "opaque" target, the emissivity adds the reflectivity equal to 1 under local thermodynamic equilibrium [18].

For a semi-infinite homogeneous isothermal medium or untransparent target, its emissivity can be given by

$$e(\theta; p) = T_B(\theta; p) \big/ T_g = 1 - \Gamma(\theta; p) \tag{1}$$

where, θ is the observation angle, $p = h$ or v, h and v denote the horizontal and vertical polarization respectively, T_B is the target radiation brightness temperature, T_g is the physical temperature of target, Γ is the reflectivity of targets. In accordance with Fresnel's law, considering that the materials are nonmagnetic material, the radiation brightness temperature of flat and untransparent targets

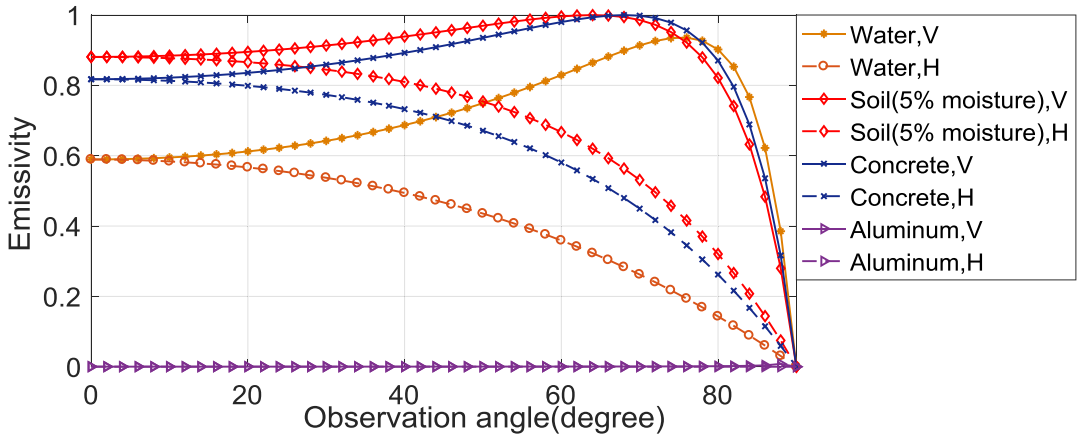

Fig. 1. Theoretical emissivities of several materials. H and V denote horizontal and vertical polarization respectively.

can be given by

$$T_B(\theta; h) = \left(1 - \left|\frac{\cos\theta - \sqrt{\varepsilon - \sin^2\theta}}{\cos\theta + \sqrt{\varepsilon - \sin^2\theta}}\right|^2\right) * T_g$$
$$T_B(\theta; v) = \left(1 - \left|\frac{\varepsilon\cos\theta - \sqrt{\varepsilon - \sin^2\theta}}{\varepsilon\cos\theta + \sqrt{\varepsilon - \sin^2\theta}}\right|^2\right) * T_g \quad (2)$$

where, ε is the permittivity of the material. From Eq. 2, surface emissivity mainly depends on the permittivity, the surface temperature, the observation angle and the polarization state.

Using Eq. 2, the emissivity of several materials under different observation angles are calculated in 94 GHz, which are shown in Fig. 1. According to the results, there are obvious differences on the polarization emissivities of these materials. The emissivities of aluminum are close to 0 under almost all observation angles, and this is also a common feature of metal materials. For non-metallic materials, the vertical polarization emissivities are usually larger than the horizontal polarization emissivities. In particular, in the Brewster angle, the vertical polarization emissivity of non-metallic materials reaches the maximum value closing to 1.0.

For PMMW imagery, when ignoring sensor effects and transmission, the apparent temperature detected by radiometer at a single point can be expressed as

$$T_{AP}^{h,v}(x, y) = [1 - e^{h,v}(x, y)]T_{amb}(x, y) + e^{h,v}(x, y)T_g(x, y) \quad (3)$$

where, $T_{AP}(x, y)$ is the apparent temperature of the corresponding pixel; x and y are the coordinates of the image; $e(x,y)$ is the emissivity of object surface in corresponding pixels, which is dependent on the polarization state and the observation angle, h and v denote the horizontal and vertical polarization respectively, T_{amb} is the ambient BT incident on the object at the reflection angle, T_g is the physical temperature of object surface in corresponding pixels.

From Eq. 3, we can know that $T_{AP}(x, y)$ depends not only on the emissivity of the object, but also on the ambient radiation and the physical temperature of target, therefore, it's not a stable value. As such, the category of the target in the image cannot be accurately identified by the $T_{AP}(x, y)$.

In this paper, to remove the influence of the ambient radiation and the physical temperature, PDoP is defined as:

$$\text{PDoP} = (T_{AP}^v - T_{AP}^h)/(2T_g - (T_{AP}^v + T_{AP}^h)) \quad (4)$$

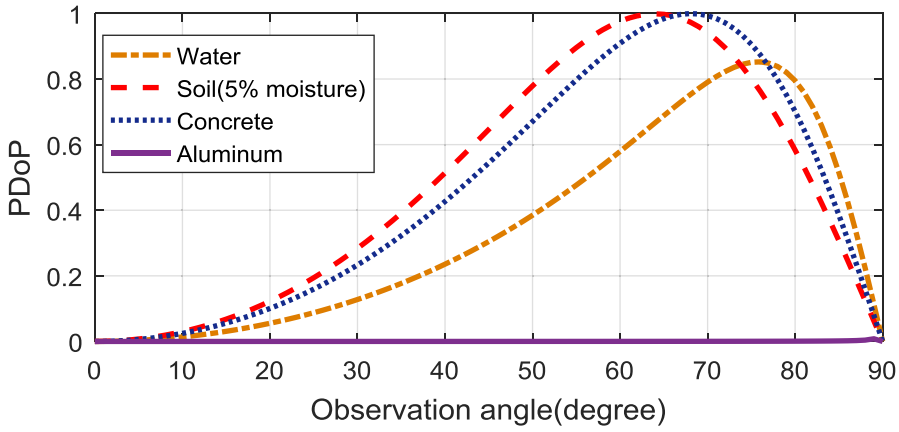

Fig. 2. Theoretical PDoP values of several materials.

In outdoor scenes, T_{amb} also comes from the sky radiation which can be considered to be unpolarized in the millimeter-wave bands. By connecting Eqs. 2 and 3, PDoP can be expressed as

$$\mathrm{PDoP} = (e_v - e_h)/(2 - (e_v + e_h)) = (\Gamma_h - \Gamma_v)/(\Gamma_h + \Gamma_v) \tag{5}$$

PDoP values range from 0 to 1, and reach the maximum at Brewster angle. For metals (e.g., aluminum), PDoP remains close to 0 at all incident angles. Eq. 5 shows that the PDoP of a target is an invariant value all day long that is only related to the target emissivity, and it may be a new feature discriminator that can be used for target clustering and recognition. For the materials involved in Fig. 1, the PDoP values are calculated and shown in Fig. 2, The calculated results indicate that there are significant differences in PDoP of these materials under almost all observation angles.

3. Experimental Details

3.1 Receiver Design and Characteristics

The receiver used in this experiment is a scanning polarimetric imaging radiometer which has been designed as a two-polarization receiver system, working at 94 GHz with 4 GHz bandwidth. The sensitivities of the receiver are approximately 0.5 K for the BT under both vertical and horizontal polarization measurement, and the noise coefficient is less than 5.5 dB. In order to obtain high main-beam efficiency, a Cassegrain antenna with a 600 mm projected aperture is used in this system. Thermal radiation is received by the dual-polarized horn antenna and is separated into two linear orthogonal polarization components by the orthomode transducer (OMT). The measured half-power beam widths are 0.4°. Visible imagery was obtained through a camera mounted on top of the system. The viewing angle of the visible and PMMW images is slightly different due to the different placements of the sensors.

The scene is scanned in two dimensions with an elevation-azimuth scanner configuration. The angular resolutions of the elevation and the azimuth drive are 0.005°, which are more than 20 times better than the half-power beam width of the antenna (0.37°), allowing for very precise positioning. The rotation ranges of the elevation and the azimuth are –45°∼+90° and –90°∼+90° respectively. Measurement points are taken in every resolution step during continuous antenna movement. The system is shown in Fig. 3.

3.2 Experiment Design

In order to verify the effectiveness of PDoP in material clustering, an outdoor experiment was designed and conducted. The visible image of the imaging scene is shown in Fig. 4, The ground is divided into four regions: the cistern (Area 1), the soil belt (Area 3), the concrete pavement (Area 2)

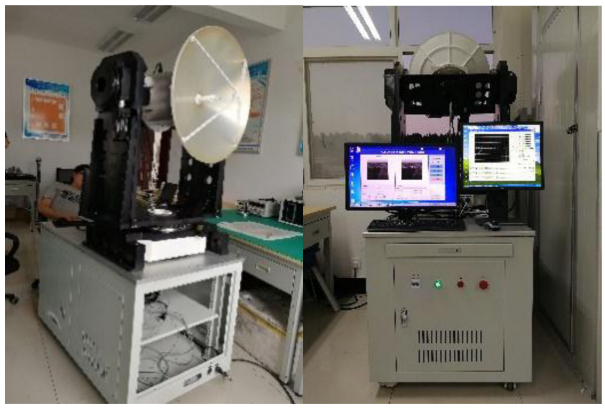

Fig. 3. Passive millimeter-wave imaging system.

Fig. 4. The visible image of the imaging scene.

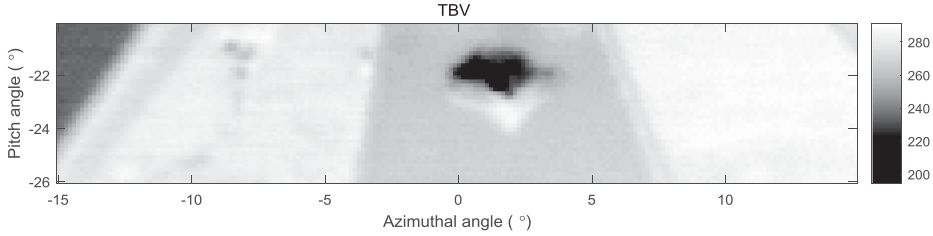

Fig. 5. Brightness temperature image of vertical polarization.

and the reserved area (Area 4). The Area 4 is not involved in the discussion of the experimental results. An airplane scaled model marked by blue solid line which is made of aluminum is placed on the cement road to simulate the real scenes, and the model is covered with rain cloth. A mini weather station is built on the reserved area.

In the measurement, the height of the radiometer is about 18 m away from the ground, the distance between the imaging area and the radiometer ranges from 20 m to 28 m, and the scanning step is 0.15°. The scan range of elevation angle is from $-20°\sim-26°$ and of the azimuth angle is from $-15°\sim+15°$. The cold and heat sources calibration method is used to calibrate the cross polarized channel of the radiometer respectively.

Figs. 5 and 6 show the horizontal and vertical polarization BT images respectively. For dielectric regions, vertical polarization BT (TBV) is larger than horizontal polarization BT (TBH). However, TBV is approximately equal to TBH for metal regions, regardless of material edge regions. Overlooking the ground surface, the emission source reflected by metals is usually the “cold” sky that can be considered as non-polarization. Hence, the TB of metals is generally small than that of terrain

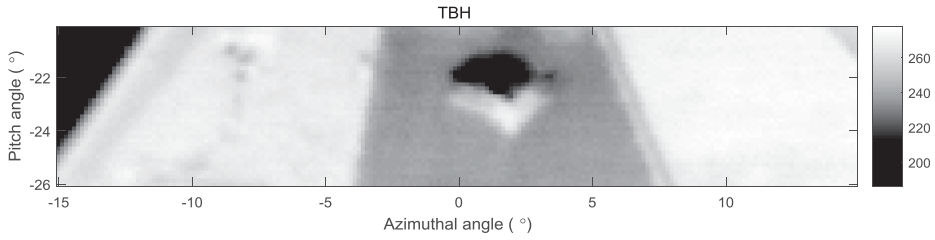

Fig. 6. Brightness temperature image of horizontal polarization.

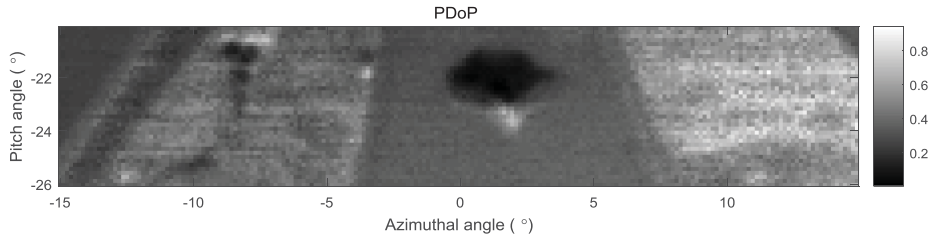

Fig. 7. PDoP image.

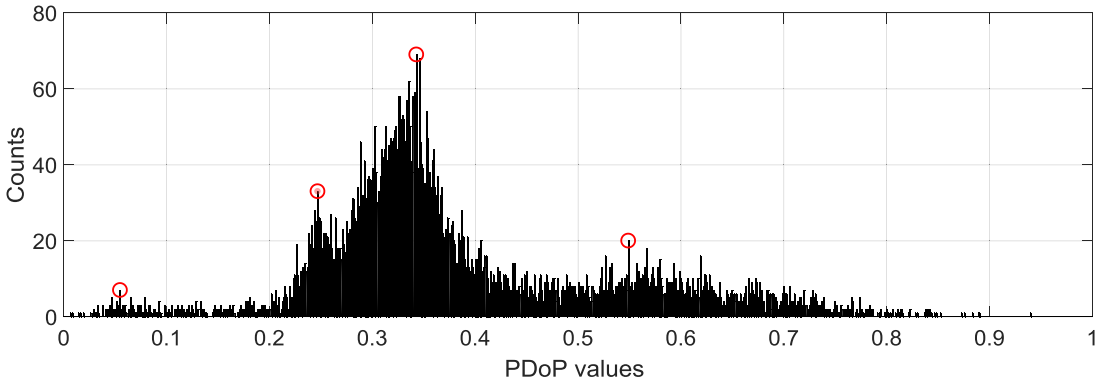

Fig. 8. The corresponding histograms for the PDoP image.

dielectrics (e.g., soil and grass). However, this deduction is not always true since the surface of a metal target may have multiple normal vector directions [12]. In Fig. 6, since the complex surface orientations lead to that the apparent temperatures of airplane model mainly come from the reflection of the low elevation sky radiation, the BT of water surface is close to that of the airplane model.

According to Eq. 4, PDoP values can be calculated with T^h_{AP}, T^v_{AP}, and T_g, of which T^h_{AP} and T^v_{AP} can be measured by radiometer, and T_g is measured by an infrared thermometer. The PDoP distribution image is shown in Fig. 7.

4. Automatic Assignment of Thresholds

Based on the theoretical analysis in Section 2, PDoP is an intrinsic quantity that has nothing to do with physical temperature and unpolarized ambient radiation. As a consequence, the PDoP is only dependent on the reflectivity under typical outdoor scenes. Therefore, it is sufficient to focus on the behavior of the PDoP to make a basic material clustering.

The histogram of the PDoP image of scene is shown in Fig. 8. Let the pixels of the PDoP image be represented in 1000 PDoP levels. The numbers of pixels at level i ($i = 1, 2 \ldots 1000$) is denoted by N_i. The data levels are divided into c clusters, and c is determined by number of extreme maximum

TABLE 1
The Boundaries and Mean PDoP Values of Each Cluster

Cluster labels	thresholds	Mean **PDoP** values of clusters
1	PDoP< 0.177	0.0976
2	0.177<PDoP < 0.265	0.2395
3	0.265< PDoP < 0.369	0.3219
4	PDoP>0.369	0.5281

points. The extreme maximum points are obtained by search algorithm and marked in Fig. 8 by red rings. From left to right, the levels corresponding to the interval maximum points are represented by I_1, I_2, I_3, I_4 respectively. According to the number of extreme maximum points, the image region can be divided into four clusters, namely C_1, C_2, C_3, C_4. Then, three thresholds X_m ($m = 1, 2, 3$) that respectively lie in the interval (I_m, I_{m+1}) are required.

For the class C_t ($t = 1, 2, 3, 4$), the within-class distance [19] can be expressed as

$$J_w = \sum_{i=K_{m-1}}^{K_m} \|N_i - e_m\|^2 \Big/ K_m - K_{m-1} + 1 \tag{6}$$

where, e_m is the mean value of the elements in the class which can be solved as

$$e_m = \frac{1}{K_m - K_{m-1}} \sum_{i=K_{m-1}+1}^{K_m} N_i, m = 1, 2, 3 \tag{7}$$

where, K_m is the level corresponding to the X_m, and $K_0 = 1$. Through Eq. 6, the extreme minimum value of J_w is taken as the criterion to search K_m between the interval (I_m, I_{m+1}). The PDoP value corresponding to the K_m level is the mst threshold X_m.

According to the results of threshold segmentation and PDoP distribution characteristics of each material, the image region is divided into four clusters. The boundaries and the mean PDoP values of each cluster are shown in Table 1.

From Table 1, by obtaining the thresholds, the image region is partitioned into four clusters. Referring to our simulation results in Fig. 2, the expected PDoP values of the metal, water, concrete and soil rank from small to large. Then the material types of the clusters with labels from 1 to 4 are metal, water, concrete and soil respectively. Because of the roughness of the surface of soil belt and the distribution of vegetation on the area, the PDoP values reflect a large distribution interval in soil region.

5. Results

To perform the clustering, we investigate the PDoP value of each pixel, and compare the results with the boundary to determine the clusters. The procedure is done for every single pixel in the image. Comparing the mean values of each cluster with the theoretical PDoP values of each material, the material types of each cluster can be determined. If the PDoP value is less than 0.177, the regarded pixel is marked as metal. If the PDoP value is between 0.177 and 0.265, the regarded pixel is marked as water. If the PDoP value is between 0.265 and 0.369, the regarded pixel is marked as concrete, if the PDoP value is bigger than 0.369, the regarded pixel is marked as soil. The results are depicted in Figs. 9–12.

Fig. 9. Classification result. The black implies metal while the gray is others.

Fig. 10. Clustering result. The black implies water while the gray is others.

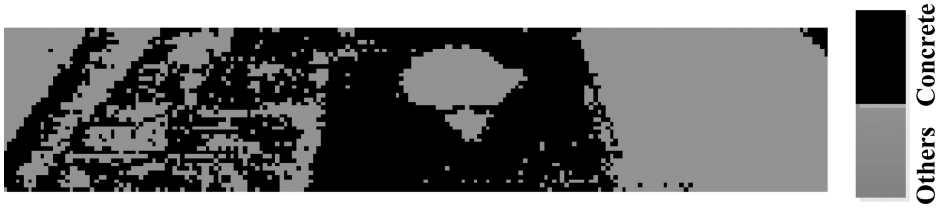

Fig. 11. Clustering result. The black implies concrete while the gray is others.

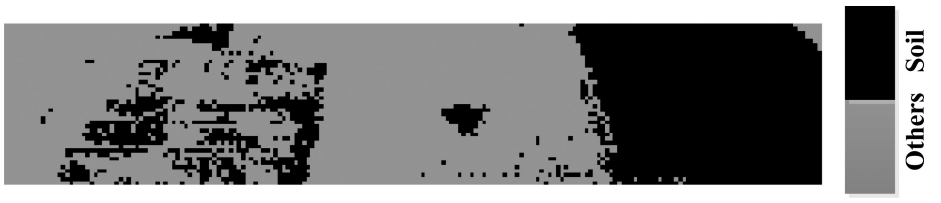

Fig. 12. Clustering result. The black implies soil while gray is others.

As shown in Fig. 9, metal and dielectric image regions are segmented by using the clustering criterion in Table 1, and the aircraft model area is effectively identified from the whole image region. The pixels in area 4, which are designated as metals, come from some metal facilities. In Fig. 10, the water area is distinguished from the whole image region, and the error pixels mainly come from two regions: one is the interface of two areas with different materials, and the PDoP value of the target region is between the PDoP values of the two areas, which results in that the PDoP values of some pixels in this region close to the PDoP values of target area. The other is the shadow area in Fig. 4, and the pixels in this area reflect the polarized radiation of the surrounding buildings rather than the polarized sky radiation. In Fig. 11, the regions covered with concrete are separated from the image region, and the error pixels mainly come from reserved area because of the vegetation and roughness and some cement buildings. The soil area is identified in Fig. 12, and the aircraft head which is made of dielectric materials leads to some error pixels.

Both the simulation results and the measurement experiment results have demonstrated that the PDoP is an effective feature discriminator that can be used for material clustering.

6. Conclusion

In this paper, a polarization-based material clustering technique using passive millimeter-wave polarimetric imagery is proposed. A feature discriminator PDoP which is sensitive to material type is introduced for removing the reflected ambient unpolarized radiation effect. Several common natural and artificial materials are selected to investigate their PDoP characteristics. Theoretical analysis shows that there are obvious differences in the PDoP characteristics of these materials. An outdoor imaging experiment is conducted to validate the presented material clustering technique, and there are water, soil, concrete and a metal aircraft model in the experimental scene. The results show that the method we proposed can identify the category of most pixels accurately in the imaging region.

Some pixels are judged erroneously due to the reasons mentioned above. Studies working on eliminating these errors will be conducted in the future. Moreover, the effect of water wave and soil vegetation on the PDoP will also be analyzed in the future.

Acknowledgment

The authors would like to thank the editor and the anonymous reviewers for their valuable suggestions.

References

[1] T. J. Hewison, "Airborne measurements of forest and agricultural land surface emissivity at millimeter wavelengths," in *Proc. Int. Symp. Geosci. Remote Sens.*, 2001, pp. 2417–2419.
[2] P. E. Racette, L. R. Dod, J. C. Shiue, and R. F. Adler, "Millimeter-wave imaging radiometer for cloud, precipitation and atmospheric water vapor studies," in *Proc. Int. Symp. Geosci. Remote Sens.*, 1992, pp. 1426–1428.
[3] A. Tait, D. Hall, J. Foster, A. Chang, and A. Klein, "Detection of snow cover using millimeter-wave imaging radiometer (MIR) data," *Remote Sens. Environ.*, vol. 68, pp. 53–60, 1999.
[4] S. E. Clark, J. A. Lovberg, C. A. Martin, and V. G. Kolinko, "Passive millimeter-wave imaging for airborne and security applications," *Proc. SPIE-Int. Soc. Opt. Eng.*, vol. 5077, pp. 16–22, 2003.
[5] B. Kapilevich, B. Litvak, A. Shulzinger, and M. Einat, "Portable passive millimeter-wave sensor for detecting concealed weapons and explosives hidden on a human body," *IEEE Sensors J.*, vol. 13, no. 11, pp. 4224–4228, Nov. 2013.
[6] W. L. Stewart, "Passive millimeter wave imaging considerations for tactical aircraft," *IEEE Aerosp. Electron. Syst. Mag.*, vol. 17, no. 12, pp. 11–15, Dec. 2002.
[7] A. Visnansky *et al.*, "Modeling passive millimeter wave imaging sensor performance for discriminating small watercraft," *Appl. Opt.*, vol. 49, pp. 58–66, 2010.
[8] L. Yujiri and M. Shoucri, "Passive millimeter wave sensors for detection of buried mines," *Proc. SPIE-Int. Soc. Opt. Eng.*, vol. 2496, pp. 2–6, 1995.
[9] J. Su, Y. Tian, F. Hu, L. Gui, Y. Cheng, and X. Peng, "An equivalent method of mixed dielectric constant in passive microwave/millimeter radiometric measurement," *Proc. SPIE-Int. Soc. Opt. Eng.*, vol. 10439, 2017, Art. no. 104390F.
[10] V. Thilak, C. D. Creusere, and D. G. Voelz, "Passive polarimetric imagery based material classification for remote sensing applications," in *Proc. Southwest Symp. IEEE Image Anal. Interpretation*, 2008, pp. 153–156.
[11] V. Thilak, D. G. Voelz, and C. D. Creusere, "Polarization-based index of refraction and reflection angle estimation for remote sensing applications," *Appl. Opt.*, vol. 46, pp. 7527–7536, 2007.
[12] Y. Cheng, F. Hu, L. Gui, L. Wu, and L. Lang, "Polarization-based method for object surface orientation information in passive millimeter-wave imaging," *IEEE Photon. J.*, vol. 8, no. 1, pp. 1–12, Feb. 2016.
[13] C. D. Creusere, K. Mehta, and D. G. Voelz, "Model-based estimation of surface geometry using passive polarimetric imaging," in *Proc. Int. Symp. Geosci. Remote Sens.*, 2010, pp. 4557–4560.
[14] L. B. Wolff, "Polarization-based material classification from specular reflection," *IEEE Trans. Pattern Anal. Mach. Intell.*, vol. 12, no. 11, pp. 1059–1071, Nov. 1990.
[15] J. S. Tyo, D. L. Goldstein, D. B. Chenault, and J. A. Shaw, "Review of passive imaging polarimetry for remote sensing applications," *Appl. Opt.*, vol. 45, pp. 5453–5469, 2006.
[16] J. P. Wilson, D. L. K. Eng, S. T. Kozacik, D. W. Prather, C. A. Schuetz, and T. E. Dillon, "Display of polarization information for passive millimeter-wave imagery," *Opt. Eng.*, vol. 51, 2012, Art. no. 091607.
[17] F. Hu *et al.*, "Polarization-based material classification technique using passive millimeter-wave polarimetric imagery," *Appl. Opt.*, vol. 55, pp. 8690–8697, 2016.
[18] F. T. Ulaby, R. K. Moore, and A. K. Fung, *Microwave Remote Sensing: Active and Passive, Volume 1 - Microwave Remote Sensing Fundamentals and Radiometry*. Norwood, MA, USA: Artech House, 1981.
[19] S. Theodoridis and K. Koutroumbas, *Pattern Recognition*, 3rd ed. San Francisco, CA, USA: Academic, 2006.